Single-cell atlas of BAL from preschool cystic fibrosis reveals key inflammatory pathways modified by the CFTR modulator ivacaftor in the early life lung.

Jovana Maksimovic[1,2,9*], Shivanthan Shanthikumar[2,3,4*], George Howitt[1,9], Gunjan Dixit[1,9], Peter F Hickey[5,6], Casey Anttila[5], Daniel V. Brown[5], Anne Senabouth[7,8], Daniela Amann-Zalcenstein[5], Joseph E. Powell[7,8], Sarath C. Ranganathan[2,3,4], Alicia Oshlack[1,9,10], Melanie R. Neeland[2,3#].

[1] Computational Biology Program, Peter MacCallum Cancer Centre, Parkville, VIC, Australia
[2] Respiratory Diseases, Murdoch Children's Research Institute, Parkville, VIC, Australia
[3] Department of Paediatrics, University of Melbourne, Parkville, VIC, Australia
[4] Respiratory and Sleep Medicine, Royal Children's Hospital, Parkville, VIC, Australia
[5] Cellular Genomics Projects Team, Advanced Technology and Biology Division, WEHI, Parkville, VIC, Australia
[6] Department of Medical Biology, University of Melbourne, Parkville, VIC, Australia
[7] Garvan-Weizmann Centre for Cellular Genomics, Garvan Institute of Medical Research, Sydney, NSW, Australia
[8] UNSW Cellular Genomics Futures Institute, University of New South Wales, Sydney, NSW, Australia
[9] Sir Peter MacCallum Department of Oncology, University of Melbourne, Parkville, VIC, Australia
[10] School of Mathematics and Statistics, University of Melbourne, Parkville, VIC, Australia

*Contributed equally
[#]Corresponding author

Corresponding author details:
Dr Melanie Neeland, PhD
Royal Children's Hospital, 50 Flemington Road, Parkville, VIC, Australia
Email: melanie.neeland@mcri.edu.au

Author contributions: JM, SS, SCR, AO and MRN designed the study. SS and SCR recruited the patients and collected samples. SS, CA, DVB, and MRN performed experiments and acquired the data. JM, SS, GH, GD, PFH, AS, AO and MRN analysed the data. JM, SS, DA-Z, JEP, SCR, AO and MRN interpreted the data. All authors edited, revised, and approved the final manuscript.

Funding: The authors would like to acknowledge funding support from the Chan Zuckerberg Initiative (Inflammation Network), National Health and Medical Research Council of Australia Synergy Grant (1183640), Investigator Grant to AO (GNT1196256), Investigator Grant to JM (2023/GNT2026098), and a Vertex Mentored Research Innovation Award. S.S is supported by a clinician-scientist fellowship from the Melbourne Children's Campus.

Acknowledgements: The authors thank the children and parents who participated in the AREST-CF study. The authors thank the CWCCG cellular genomics team and the WEHI SCORE team.

Conflict of interest: The authors have no conflicts of interest to declare

ABSTRACT

Aberrant inflammation and structural lung damage occurs early in life for people with cystic fibrosis (CF). Even in the era of CFTR modulators, anti-inflammatory therapy may still be needed to prevent establishment and lifelong consequences of bronchiectasis. In this study, we integrated transcriptome-wide single-cell RNA sequencing data, highly multiplexed surface protein expression, and functional pathway analysis to create a comprehensive paediatric lower airway atlas of 44 immune and epithelial cell populations in bronchoalveolar lavage (BAL). We then analysed this atlas to investigate inflammatory cell responses in children with CF to show widespread dysregulation of macrophage function in the preschool CF lung. This included alterations in pathways associated with SARS-COV and influenza responses, TNF/IFN signalling, cholesterol homeostasis, and pulmonary fibrosis that were further altered by the early development of bronchiectasis. We showed that the CFTR modulator ivacaftor restores some of these macrophage-related functional deficits and reduces expression of pathways associated with neutrophil infiltration, however the modulator lumacaftor/ivacaftor was not associated with any detectable change in transcriptional response. This work represents a comprehensive, multi-omic single-cell analysis of bronchoalveolar lavage from preschool children and the results inform the future development of anti-inflammatory therapy for children with CF.

INTRODUCTION

For people with cystic fibrosis (CF), the preschool years are key to realising the goal of living a life unaffected by the disease. This is because irreversible structural lung disease frequently develops in this period [1]. Once that has occurred, even if cystic fibrosis transmembrane conductance regulator (CFTR) dysfunction is corrected, via either CFTR modulators or novel approaches such as gene therapy, people with CF will still have to manage the lifelong consequences of bronchiectasis [2]. Inflammation is a key driver of the development of early life structural lung disease in CF, with pulmonary inflammation being the strongest contributor to the development of structural lung disease in early life CF [3]. Despite this, there are no anti-inflammatory treatments used in practice which prevent structural lung disease. For preschoolers with CF not taking modulator therapy, either due to ineligible *CFTR* genotypes, inability to access the medication, or inability to tolerate modulators due to adverse effects, the potential benefit of effective anti-inflammatory therapy is clear. There may also be a need for synergistic anti-inflammatory therapy in those receiving modulator therapy as some studies have found that inflammation persists even when they are used [4].

A better understanding of the mechanisms of aberrant pulmonary inflammation in preschool children with CF is needed to identify targets for anti-inflammatory therapy. While neutrophilic inflammation is associated with the development of structural lung disease and commonly studied in CF [5] , determining the role of other inflammatory cell types and immunological processes that lead to the establishment of pathogenic neutrophil-dominated inflammation is crucial for developing effective anti-inflammatory therapies.

Single cell RNA-sequencing (scRNA-seq) allows profiling of cell composition and function at an unprecedented resolution. Previous studies employing this technique on lung samples from people with CF have not included preschool children and have focused predominantly on epithelial samples [6]. In this study, we aimed to use scRNA-seq combined with antibody derived tags (ADTs) (CITE-seq) to develop a comprehensive single-cell atlas of the early life airway and extensively profile inflammation in bronchoalveolar lave (BAL) samples collected from preschool children with CF (both treated and untreated with CFTR modulators, and with and without bronchiectasis) as well as age-matched non-CF controls, to inform the future development of anti-inflammatory therapy.

RESULTS

1. An immune and epithelial cell atlas of early life BAL

This study includes scRNA-seq analysis of 45 BAL samples from children with CF and non-CF controls (Extended Data File 1, Figure 1A). The CF group consisted of children who had surveillance bronchoscopy as part of clinical care [5], and the control group were children who underwent general anaesthesia for assessment of upper airway disease (i.e. stridor). For children with CF, metadata were recorded including treatment with modulator therapy (ivacaftor or lumacaftor/ivacaftor) and presence or absence of bronchiectasis. Single-cell RNA sequencing of BAL samples was performed using the 3' 10x Genomics Chromium platform, either with or without the addition of ADTs (BioLegend TotalSeqA Human Universal Cocktail v1.0). Details of the bioinformatic analysis undertaken are provided in the methods and supplement, and the complete analysis is available at https://oshlacklab.com/paediatric-cf-inflammation-citeseq/index.html with additional data tables available at https://github.com/Oshlack/paediatric-cf-inflammation-citeseq/tree/main/output/dge_analysis

Unsupervised clustering of scRNAseq data and cell annotation using marker gene analysis revealed 16 transcriptionally distinct broad cell populations in paediatric BAL representing all of the expected cell types (Figure 1B-C). Marker genes for each broad cell population are shown in Figure 1D. These marker genes included those described previously for well characterised lineages [7,8]. We also observed three subsets of proliferating cells (annotated proliferating T/NK, proliferating macrophages and dividing innate cells) which expressed known proliferation genes including *TOP2A*, *MKI67*, *STMN1*, and *TUBB*. The annotations of each cell population were further confirmed by analysis of expression of TotalSeq-A ADTs (Figure 1E).

2. Sub-clustering analysis reveals heterogeneity within BAL macrophages, T cells, myeloid cells, and other rare cell populations.

As macrophages are the most abundant immune cell in BAL, we performed a sub-clustering analysis of our broad macrophage population. This revealed 17 subpopulations with distinct transcriptional signatures (Figure 2A-C). Eight of these have been previously reported in studies from adult lung samples [7,9]. We also show five subpopulations of macrophages that can be defined based on expression of *IFI27* and *APOC2*, two key genes shown in a recent

study to define macrophage populations in healthy BAL [9]. We identified *IFI27+* macrophages (macro-IFI27), *IFI27+* macrophages with upregulation of *CCL18* (macro-IFI27+CCL18+), macrophages positive for both *IFI27* and *APOC2* (macro-IFI27+APOC2+), *APOC2+* macrophages (macro-APOC2+) as well as a subset of macrophages expressing *APOC2+* as well as lipid transport associated genes (macro-lipid-APOC2+). We identified a subset of macrophages enriched for insulin growth factor 1 (*IGF1*) (macro-IGF1), and another subset of macrophages showing evidence of T cell interaction based on marker genes (*CCL5, IL32, CD2*) and protein expression. It is possible that these macro-T cells represent doublets, however a growing body of evidence using a variety of methods have suggested that biologically meaningful insights into cellular interactions could be gained from these populations [10-13]. Finally, we show proliferating macrophages, which were separated further based on their cycling stage: G2M phase (macro-proliferating-G2M) and S phase (macro-proliferating-S). Protein expression on each of these macrophage populations is shown in Supplementary Figure 2A.

As with macrophages, we next explored heterogeneity within T/NK subsets which revealed 14 subpopulations with distinct transcriptional signatures, 11 of which have previously been reported (Figure 2D-F) [7,8]. We further show 3 subsets of activated T cells, which were annotated based on marker genes as well as REACTOME pathway analysis, one expressing *NFκB* related genes and pathways (CD4 T-NFκB), one expressing *IFN* related genes and pathways (CD4 T-IFN), and one expressing inflammasome activated genes and pathways (CD8 T-inflammasome). These inflammatory T cells were observed in both the healthy control and children with CF (Figure 2F). Protein expression on each of these T/NK populations is shown in Supplementary Figure 2B.

A final sub-clustering analysis of all other cells (not macrophages, not T/NK) revealed further heterogeneity within the rarer monocyte, DC, B cell and epithelial cell clusters (Figure 2G-I). DCs were separated into conventional DC (cDC1 and cDC2), plasmacytoid DC, and migratory DC, based on previously described marker genes and protein expression. Plasma B cells were also identified, characterised by key marker genes (*MZB1, TNFRSF17)* as well as protein expression of plasma markers CD27 and CD38. A rare subset of B cells expressing heat shock proteins (HSP) was also identified in our data, characterised by expression of HSP genes *HSPA1B, HSPA6, HSPB1* and enrichment of REACTOME pathways associated with

heat shock response. This subset of B cells has recently been described in a single-cell sequencing study of rheumatoid arthritis [14]. We identified 2 subtypes of airway epithelial cells: ciliated epithelial cells and secretory epithelial cells. Protein expression on each of these rare cell populations is shown in Supplementary Figure 2C.

3. Widespread dysregulation of BAL macrophage responses in preschool children with CF compared to non-CF controls.

We firstly compared BAL immune cell proportions between children with CF (not on any modulator therapy) (CF.NO_MOD) (n=25) and non-CF controls (n=8). Given that out BAL samples are comprised of >80% macrophages, we examined macrophages subtype proportions as a fraction of total macrophages, whilst proportions of T/NK and rare cells were examined relative to the total pool of T/NK and rare cells. This revealed that children with CF have reduced monocytes (CF.NO_MOD=0.0102, non-CF control=0.0248; p=0.009, FDR=0.001), increased NK-T cells (CF.NO_MOD=0.0042, non-CF control=0.0025; p=0.01, FDR=n.s.), increased CD4 Tregs (CF.NO_MOD=0.0173, non-CF control=0.0102; p=0.01, FDR=n.s.), and increased macro-IGF1 cells (CF.NO_MOD=0.0506, NON_CF.CTRL=0.0234; p=0.001, FDR=0.0233) relative to non-CF controls (Figure 3A). We identified 518 differentially expressed genes (DEGs) between samples from children with CF_NO_MOD and non-CF controls within alveolar macrophages, monocyte-derived macrophages, macro-CCL, and macro lipid (Figure 3B). A heatmap depicting the most significant DEGs for each macrophage subpopulation is shown in Figure 3C, and a representative volcano plot depicting up and down regulated genes within the total macrophage pool is shown in Figure 3D. All DEGs across all subpopulations are provided on the analysis website. Enrichment analysis of these DEGs using the REACTOME and HALLMARK databases revealed upregulation of pathways associated with eukaryotic translation and elongation, SRP dependent co-translational protein targeting to membrane, and SARS COV-1 and -2 host translation machinery in macro-alveolar, macro-CCL and macro-lipid populations from children with CF (Figure 3E). Conversely, downregulation of pathways associated with TNFA signalling, inflammatory responses, MTORC1 signalling, and cholesterol homeostasis were observed in both alveolar and monocyte-derived macrophages from children with CF (Figure 3F). Monocyte-derived macrophages from children with CF showed downregulation of some unique pathways, including L1CAM interactions, RHO GTPASES and IL-10 signalling, which were not observed in other macrophage subpopulations (Figure 3E).

We also observed transcriptional signatures that suggest remodelling of pulmonary fibrosis pathways in CF alveolar macrophages. This was evident in multiple gene sets, including "lung fibrosis" (FDR=0.0001), "pulmonary fibrosis ctd" (FDR=0.0009), and "overview of proinflammatory and profibrotic mediators" (FDR=0.0005) (Figure 3G).

Due to their abundance in BAL, macrophage subpopulations provided the most power to detect differential gene expression and were therefore the focus of our analysis. However, we also explored differential expression within other cell types in BAL where cell numbers permitted (CD4 T cells, CD8 T cells, and dendritic cells). This showed limited differences between children with CF and controls (Supplementary Figure 3).

4. BAL macrophage transcriptional signatures are associated with CF bronchiectasis.

Within the CF.NO_MOD samples, 8 had evidence of bronchiectasis on chest CT and 17 had no evidence of bronchiectasis on chest CT. We therefore compared BAL cell proportions and differential gene expression between these two groups, where those with bronchiectasis were termed "severe" and those without bronchiectasis were termed "mild". Samples from children with mild lung disease had elevated proportions of CD4 T-IFN cells (mild=0.01439, severe=0.0057; p=0.01, FDR=n.s.) and reduced proportions of HSP+ B cells (mild=0.0026, severe=0.0091; p=0.03, FDR=n.s.) relative to samples from children with severe lung disease (Figure 4A).

When exploring differential gene expression within macrophage subpopulations, we show key differences between mild and severe lung disease within the alveolar, macro-CCL, macro-IFI27, macro-APOC2, and proliferating macrophage populations (Figure 4B, Supplementary Figure 4). In total, we identified 110 DEGs, several of which overlapped across multiple macrophage subpopulations, suggesting these genes are playing key roles in the response by these cells (Figure 4C). These included *CLIC2, SLC28A3, MMP14, VAMP5, CTSK, LILRB2, SLC46A1* and *ARPIN* which were upregulated across multiple macrophage subpopulations in severe lung disease compared to mild lung disease, and *ARHGEF5, GPD1, TLCD4, GBP3, SIRPB1* and *ITGA1* which were downregulated in multiple macrophage subpopulations in severe lung disease compared to mild lung disease (Figure 4C).

As in section 3, differential expression analysis within CD4 T cells, CD8 T cells and dendritic cells in children with CF with bronchiectasis (severe) and those without (mild) was performed and summarised in Supplementary Figure 5.

5. The CFTR modulator ivacaftor modifies BAL macrophage response in early life.

We also explored the effect of CFTR modulator therapy on early life lung inflammation by comparing responses in samples from CF children on two modulator therapies: ivacaftor (8 BAL samples) and lumacaftor/ivacaftor (4 BAL samples). Relative to CF_NO_MOD, samples from children on ivacaftor (CF.IVA) have reduced proportions of NK-T cells (CF.IVA=0.0012, CF.NO_MOD=0.0042; p=0.01, FDR=n.s.) (Figure 5A), which were elevated in CF.NO_MOD relative to non-CF controls (Figure 3A). CD4 T-IFN cells, associated with mild lung disease in our cohort (Figure 4A), tended to be elevated in CF.IVA relative to non-CF controls (CF.IVA=0.0222, CF.NO_MOD=0.0116; p=0.05, FDR=n.s.) (Figure 5A). Monocytes, which were reduced in CF.NO_MOD relative to non-CF controls (Figure 3A), remained reduced following treatment with ivacaftor (CF.IVA=0.1032, CF.NO_MOD=0.0990; p=0.02, FDR=n.s.) (Figure 5A). When exploring proportion differences induced by treatment with lumafactor/ivacaftor (CF-LUMA_IVA) we did not see a reduction in NK-T cells as we did for CF-IVA (CF.NO_MOD=0.0232, CF.LUMA_IVA=0.0014; p=0.89, FDR=n.s.) (Figure 5B). CD4 Tregs, which we showed earlier to be elevated in CF.NO_MOD relative to non-CF controls (Figure 3A), remained elevated in CF.LUMA_IVA (CF.LUMA_IVA 0.0394, CF.NO_MOD=0.0173; p=0.03, FDR=n.s.), and monocytes tended sto remain reduced (CF.LUMA_IVA=0.1150, CF.NO_MOD=0.0990; p=0.09) (Figure 5B). Similar to CF.IVA, CD4-IFN cells tended to be elevated in CF.LUMA_IVA relative to non-CF controls (CF.LUMA_IVA=0.0095, CF.NO_MOD=0.0116; p=0.06, FDR=n.s.). Relative to CF.NO_MOD, as well as compared to non-CF controls, we showed elevated proportions of the macro-CCL18 subset in CF.LUMA_IVA which was not observed in CF.IVA (CF.LUMA_IVA=0.1045, CF.NO_MOD=0.0751, NON_CF.CTRL=0.0608; p=0.01 and p=0.02, respectively, FDR=n.s.) (Figure 5B).

Differential expression analysis within macrophage populations revealed a significant effect of ivacaftor treatment (CF.IVA) on macrophage gene expression relative to CF.NO_MOD (506 DEGs in total) (Figure 5C-E). Conversely, we observed no significant differences in gene expression between lumacaftor/ivacaftor (CF.LUMA_IVA) samples and CF.NO_MOD

samples in any macrophage subpopulation, suggesting a limited effect of lumacaftor/ivacaftor on macrophage function in the CF airway. We note however the more limited numbers in the CF.LUMA_IVA group (n=4) relative to the CF.IVA group (n=8).

Enrichment analysis of CF.IVA vs CF.NO_MOD DEGs using the REACTOME and HALLMARK gene sets revealed upregulation of pathways associated with cholesterol homeostasis, androgen responses, and IFN-A responses in CF.IVA relative to CF.NO_MOD across these macrophage subpopulations. Many of these pathways were shown to be impaired and downregulated in CF children not on modulator therapy compared to non-CF controls (Figure 3). Further, eukaryotic translation was downregulated in CF.IVA relative to CF.NO_MOD across these macrophage subpopulations. These pathways were upregulated in CF children not on modulator therapy compared to non-CF controls (Figure 3). Figure 5F shows representative pathway analysis within the alveolar macrophage population, however similar responses were also observed in other macrophage subpopulations including macro-CCL and macro-lipid (see analysis website). These findings suggest that ivacaftor treatment restores some of the CF macrophage-associated functional deficits in early life.

Ivacaftor also induced remodelling of neutrophil response pathways in alveolar macrophages as highlighted by enrichment of the Gene Ontology pathways secretory granules (FDR=0.00003, 23 DEGs) and secretory vesicles (FDR=0.00003, 25 DEGs) and the REACTOME pathway neutrophil degranulation (FDR=8.45E-06, 18 DEGs) (Figure 5G). This signature was unique to the alveolar macrophage subpopulation, highlighting a key role for these cells in regulating the neutrophil response following initiation of ivacaftor. Key genes in these pathways are shown in Figure 5H, all of which were significantly downregulated (all FDR<0.05) in CF.IVA samples relative to CF.NO_MOD samples.

As a final avenue to determine the effects of ivacaftor treatment on CF macrophage associated functional deficits, we compared cell-specific gene expression in CF.IVA with that of non-CF controls. While we see substantially less differential gene expression within macrophage subpopulations between CF.IVA and non-CF controls when compared to CF.NO_MOD vs non-CF controls, we still show evidence of altered gene expression related to TNFA signalling and inflammatory response in macrophages and their subpopulations from CF.IVA children relative to non-CF controls (Supplementary Figure 6). This highlights that while ivacaftor was associated with improvements in a range of these pathways when

compared to untreated CF children, this improvement represents a partial restoration of these responses that are still significantly altered from controls.

DISCUSSION

In this study, we integrated transcriptome-wide single-cell RNA sequencing data, highly multiplexed surface protein expression, and functional pathway analysis to extensively characterise 44 immune and epithelial cell populations in early life BAL. We then analysed this extensive BAL atlas to compare transcriptional responses in samples from children with CF and non-CF controls and discovered widespread dysregulation of macrophage function in the early life CF lung, which was further altered by the early development of bronchiectasis. We showed that the CFTR modulator ivacaftor restores some of these macrophages related functional deficits, and that the modulator lumacaftor/ivacaftor was not associated with any detectable change in transcriptional response.

Previous scRNA-seq studies involving people with CF have largely characterised adult samples and primarily focused on respiratory epithelium rather than immune cells. This is also true for the broader pulmonary scRNA-seq field [8,15]. Our paediatric-specific dataset revealed several novel cell subtypes not observed in adult studies, such as CD4 T cells with NFκB and IFN activation signatures. As these cells were found in both children with CF and healthy controls, they are unlikely to be disease specific and may represent cell types specific to early life, a finding which needs external validation. The proportion of broad cell types identified differs from previous studies in that there is a low proportion of neutrophils in our work, likely due to the impact of cryopreservation [16], along with the known difficulties in detecting neutrophils using droplet based sc-RNAseq technology.

We showed dysregulation of a range of immune response pathways in four key macrophage populations (macro-alveolar, macro-monocyte derived, macro-CCL and macro-lipid) in children with CF relative to age-matched controls. This included upregulation of pathways associated with SARS-COV-1 and -2 host machinery and influenza infection (defense responses), downregulation of pathways associated with TNF/IFN signalling and cholesterol homeostasis, as well as evidence for remodelling of pulmonary fibrosis pathways. A recent study applying scRNAseq to lungs from CF and wildtype piglets revealed similar alterations in CF lung myeloid cell gene expression, including elevated pathways associated with immune defense response, reduced cytoplasmatic translation, and enrichment for S100 alarmins and matrix metalloproteinases (MMPs) [17]. This was also associated with impaired phagocytosis function, similar to previous work in sputum from adults with CF [18]. In our study, macrophages from children with evidence of bronchiectasis had higher expression of

genes such as *CLIC2, MMP14* and *CTSK*, which have been associated with pulmonary fibrosis and indeed the MMP proteins have been explored as therapeutic targets in CF lung disease [19-21]. We also showed upregulation of *LILRB2*, a negative regulator of myeloid cell activation, in early life CF bronchiectasis. Recent work has shown anti-LILRB2 therapy increases macrophage activation (*NFKB* and *STAT1*) as well as alters genes involved in lipid and cholesterol metabolism [22]. Overall, our findings and others highlight that in those not eligible for modulator therapy, where gene therapy is the next therapeutic approach being trialled, that CFTR may need to be corrected in macrophages as well as the respiratory epithelium to prevent the harms of CF-related pulmonary inflammation.

Alveolar macrophages from the ivacaftor treated group had reduced expression of genes associated with neutrophil recruitment and degranulation. Supporting this, we have previously shown ivacaftor is associated with a reduced proportion of neutrophils and reduced concentration of inflammatory cytokines in BAL [23,24], and elexacaftor/tezacaftor/ivacaftor (ETI) therapy was also recently associated with reduced expression of neutrophil recruitment pathways in macrophages obtained from nasal brushings [6]. Together these findings suggest that highly effective modulator therapy, commenced in early life, may be effective in preventing the development of neutrophil dominant inflammation. We also showed in several macrophage subsets that pathways observed to be downregulated in CF compared with non-CF controls were upregulated by ivacaftor. This included cholesterol homeostasis and interferon-A responses, indicative of an ivacaftor-induced restoration of key macrophage functions similar to that observed with ETI [6]. We showed no detectable effect of lumacaftor/ivacaftor treatment when compared to children not on modulator therapy, although we acknowledge the smaller number of participants in this cohort. This limited impact of lumacaftor/ivacaftor therapy is perhaps not surprising given the modest clinical impact of this treatment when compared to other modulator therapies [25].

This study has limitations which must be acknowledged. The cross-sectional design limits the ability to infer causality with regards to treatment effect. The fact that the control group is made up of children undergoing surgery for upper airway pathology is another limitation that reflects the difficult in obtaining BAL samples from children for research. To try and ensure the control group had no lung disease we used a parent questionnaire and excluded any participants who reported lung pathology. Further, participants treated with modulators will have been treated for different lengths of time, however as modulator therapy is associated with changes in CFTR function and clinical outcomes within 2 weeks of treatment initiation

this is unlikely to be significant [26]. New modulators, such as ETI and now vanzacaftor–tezacaftor–deutivacaftor, mean that ivacaftor and lumacaftor/ivacaftor have been superseded. However, at the time of this study these were the agents used in clinical practice in Australia and the results still offer insights into the degree of CFTR function correction needed to alter pulmonary inflammation.

This is the most comprehensive, multi-omic single-cell analysis of bronchoalveolar lavage from preschool children. These data have identified novel cell populations in the early life lung, highlighted multiple aberrant pathways leading to macrophage dysfunction in preschool CF, and demonstrated the benefits of the CFTR modulator ivacaftor at a transcriptomic level.

METHODS

Study participants

This study included 45 bronchoalveolar (BAL) samples from children with CF (n=37) and non-CF controls (n=8) (Extended Data File 1). The CF group consisted of children who had surveillance bronchoscopy as part of clinical care through the AREST-CF program [5]), and the control group were children without cystic fibrosis who underwent general anaesthesia for assessment of upper airway disease (such as stridor). Children had bronchoscopy performed at the time of clinical stability with no clinical features of acute infection. The median age of the CF participants was 3.03 years (range 0.5-6.2 years) and the median age of the non-CF controls was 2.11 years (range 0.84-8.4 years). Within the CF samples, n=25 were not on any CFTR modulator therapy, 8 were receiving the CFTR modulator ivacaftor and 4 were receiving the CFTR modulator lumacaftor/ivacaftor.

Ethics statement

This study was reviewed and approved by Royal Children's Hospital Research Ethics Committee (HREC #25054). Written informed consent to participate in the studies was provided by the participants' legal guardian/next of kin.

Bronchoalveolar lavage procedure and processing of samples

Three aliquots of sterile normal saline (1mL/kg, max 20mL per aliquot) were instilled into the right middle lobe and another lavage of an aliquot was performed in the lingula or the site of greatest disease. This study used BAL from aliquots two and three from the right middle lobe. BAL was assessed for infection as per standard clinical testing in the RCH clinical microbiology laboratory. BAL samples were processed according to our openly available protocols [27]. In brief, samples were immediately placed on ice and processed within 1 hour of the procedure. Samples were centrifuged at 300 x g for 7 min at 4°C. The cell pellet was resuspended in 10mL of media (RPMI supplemented with 2% fetal calf serum (FCS)), filtered through a 70uM filter and centrifuged at 300 x g for 7 min at 4°C. Supernatant was discarded and the cell pellet resuspended in media for cell counting. The sample was then centrifuged at 300 x g for 7 min and resuspended in equal parts media and chilled freezing solution (FCS with15% dimethyl sulfoxide (DMSO)). The freezing solution was added to resuspended cells drop by drop on ice. The samples were transferred to cryovials, and then cooled at −1°C per minute to −80 °C overnight before being transferred to liquid nitrogen for storage.

Collection of clinical information

Medication records were reviewed, and participants were classified as being treated or not treated with CFTR modulator therapy. At the time of the study, modulator therapies that were available to the participants were ivacaftor (IVA) (for children with an eligible class III or IV mutation), and lumacaftor/ivacaftor (LUMA/IVA) (for children homozygous for Phe508 del mutation). Children not on modulator therapy either had a genotype ineligible for modulator therapy, or their parents had elected not to start treatment. To assess lung disease severity, each participants most recent computed tomography scan was reviewed by a clinician trained in the assessment of early life CF scans, and participants were classified as having bronchiectasis (herein denoted severe lung disease) or not (herein denoted mild lung disease).

Processing of BAL samples for single-cell sequencing

Cryopreserved BAL cells were thawed in 10mL media (RPMI supplemented with 10% heat-inactivated FCS) with 25U/mL benzonase at 37°C and centrifuged at 300 x g for 10 min. The pellet was resuspended in 1mL PBS for cell counting. Following cell count, 9mL PBS was added to the tube and cells were centrifuged at 300 x g for 10 min. Supernatant was discarded and the cell pellet resuspended in PBS for viability staining using live/dead fixable near infrared viability dye (Invitrogen) according to manufacturers' instructions. The viability dye reaction was stopped by the addition of FACS buffer (2% heat-inactivated FCS in PBS 2mM EDTA) and cells were centrifuged at 400 x g for 5 min. Cells were resuspended in FACS buffer for live, single cell sorting using a BD FACSAria Fusion according to the gating strategy outlined in Supplementary Figure E1. Samples were processed for single-cell sequencing in 6 batches, the first batch (samples 40.1-43.1) were processed for single-cell RNA sequencing (without the addition of ADT's) using the "scRNAseq protocol" below, and the remaining 5 batches (samples 1.1-39.2) were processed for CITE-seq using the "CITEseq protocol" below.

scRNA-seq protocol

Sorted cells were counted and assessed for viability with Trypan Blue using a Countess automated counter (Invitrogen) and then resuspended at a concentration of 800-1000 cells/μL (8×105 to 1×106 cells/mL). Final cell viability estimates ranged between 92-96%. Single cell suspensions were loaded onto 10X Genomics Single Cell 3' Chips along with the reverse transcription (RT) mastermix as per the manufacturer's protocol for the Chromium Single

Cell 3' Library (10X Genomics; PN-120233), to generate single cell gel beads in emulsion (GEMs). Reverse transcription was performed using a C1000 Touch Thermal Cycler with a Deep Well Reaction Module (Bio-Rad) as follows: 55°C for 2h; 85°C for 5min; hold 4°C. cDNA was recovered and purified with DynaBeads MyOne Silane Beads (Thermo Fisher Scientific; Cat# 37002D) and SPRIselect beads (Beckman Coulter; Cat# B23318). Purified cDNA was amplified as follows: 98°C for 3min; 12x (98°C for 15s, 67°C for 20s, 72°C for 60s); 72°C for 60s; hold 4°C. Amplified cDNA was purified using SPRIselect beads and sheared to approximately 200bp with a Covaris S2 instrument (Covaris) using the manufacturer's recommended parameters. Sequencing libraries were generated with unique sample indices (SI) for each chromium reaction. Libraries for all samples were multiplexed and sequenced across on 2×150 cycle flow cells on an Illumina NovaSeq 6000 (26bp (Read 1), 8bp (Index), and 98 bp (Read 2)).

The Cell Ranger Single Cell Software Suite (version 6.0.2) by 10x Genomics was used to process raw sequence data into FASTQ files and read counts per cell, per gene. First, raw base calls from multiple flow cells were demultiplexed into separate pools of samples. Reads from each pool were then mapped to the GRCh38/hg38 genome (version 12) using STAR.

CITE-seq protocol

Sorted live single cells were centrifuged at 400 x g for 5min at 4°C and resuspended in 25µL of cell staining buffer (BioLegend). Human TruStain FcX FC blocking reagent (BioLegend) was added according to manufacturers' instructions for 10min on ice. Each tube was made up to 100µL with cell staining buffer and TotalSeq Hashtag reagents (BioLegend) were added to each sample for 20min on ice. Cells were washed with 3mL cell staining buffer and centrifuged at 400xg for 5min at 4°C. Supernatant was discarded and each sample resuspended at 62,500 cells/100µL following which 100µL of each sample were pooled into one tube. Pooled cells were centrifuged at 400xg for 5min at 4°C, supernatant discarded, and resuspended in 25µL cell staining buffer and 25ul of TotalSeqA Human Universal Cocktail v1.0 (BioLegend) for 30min on ice. Cells were washed in 3mL cell staining buffer and centrifuged at 400xg for 5min at 4°C. Following two more washes, cells were resuspended in PBS + 0.04% BSA for Chromium captures. Single-cell captures and library preparations were processed with the 10x Genomics Chromium single-cell Platform using the 10x Chromium Next GEM single-cell 3' Reagent V3.1 Dual Index kits (10x Genomics, USA) following the manufacturer's manual, where each pool was run on two captures to maximise cell numbers.

The barcoded cDNA was PCR-amplified and scRNA-seq libraries were constructed using the 10x 3'v3.1 library kits. The TotalSeq-A scADT-seq and scHTO-seq libraries were constructed as per manufacturer's instructions (BioLegend). The duplicate scRNA-seq, scADT-seq and scHTO-seq libraries were quantified by Tapestation 4200 D1000 chip (Agilent). Upon input normalisation, the libraries were pooled and sequenced on the Illumina NextSeq500 sequencing platform. Reads from each sample were processed using 10x Genomics Cell Ranger software (version 5.0.0). 'cellranger mkfastq' was used to demultiplex the Illumina sequencer's BCL files into FASTQ files. Next, 'cellranger count' was used to generate single-cell gene-count matrices against the 10x Genomics pre-built GRCh38 reference genome and transcriptome (2020-A (July 7, 2020) version).

Single cell sequencing data analysis

All data analysis and visualisation was performed using the R programming language versions 4.3.2 and 4.3.3. All of the code, figures and outputs for the analyses described herein can be viewed at the following workflowr (1.7.1) [28] analysis website on GitHub: https://oshlacklab.com/paediatric-cf-inflammation-citeseq/index.html. The code, as well as all necessary inputs and outputs can be cloned from the GitHub repository associated with the analysis website: https://github.com/Oshlack/paediatric-cf-inflammation-citeseq with additional data tables available at https://github.com/Oshlack/paediatric-cf-inflammation-citeseq/tree/main/output/dge_analysis. The exact R version and all package versions corresponding to each part of the analysis are specified in the "Session Info" section of each page on the analysis website.

As the data generated for this study came from two separate experiments; a small pilot (1 batch) and a larger cohort (6 batches), when discussing parts of the analysis that are unique to each experiment they will be referred to as the "scRNA-seq" (4 samples) and "CITE-seq" (41 samples) data, respectively. The analysis approaches described herein were based on the analysis we presented in Maksimovic et al., 2022 [29] with modifications.

Quality control and sample demultiplexing

The `DropletUtils` (1.22.0) Bioconductor (3.18) package was used to read in the raw Cell Ranger counts and identify non-empty droplets for each individual capture. Droplets were deemed to be non-empty if they had FDR <= 0.001 as per the `emptyDrops` function [30]. 329,403 non-empty droplets were identified across all batches.

The "CITE-seq" samples were demultiplexed based on the hashtag oligo (HTO) counts using the Bioconductor `demuxmix` package (1.4.0) with model="naive", separately for each capture [31]. The "CITE-seq" samples were also demultiplexed using their genetic information by running `cellsnp-lite` (1.2.0) [32] and `vireo` (0.5.6) [33] . Specifically, reads from non-empty droplets were genotyped at 36.6M SNPs with minor allele frequency (MAF) > 0.0005 in the 1000 Genomes Project using `cellsnp-lite` (genome1K.phase3.SNP_AF5e4.chr1toX.hg38.vcf.gz was downloaded from https://sourceforge.net/projects/cellsnp/files/SNPlist/) and then `vireo` was used to assign each cell barcode to 1 of 8 donors, doublets, or unassigned based on these genotypes. This was run separately for each capture, and then pairs of donors were matched across captures by identifying the best match between captures based on the genotype profile of each donor.

Quality control was performed on each sample independently by visually examining the total cell number, the total unique molecular identifier (UMI) count distributions, the number of unique genes detected, and the proportions of ribosomal and mitochondrial gene counts per cell. Considering only droplets genetically assigned to a donor, outlier droplets in terms of mitochondrial read % were detected based on being more than 3 median absolute deviations (MADs) from the median value of the metric across all droplets, in each sample. Droplets that were identified as mitochondrial read % outliers were then removed, as were droplets that could not be assigned to a sample based on genetics.

To detect within-sample doublets that could not be identified from the genetic and HTO demultiplexing data, both `scds` (1.18.0) [34] and `scDblFinder` (1.16.0) [35] were used. `scds` was run in `cxds`, `bcds` and `hybrid` mode with estDbl=TRUE, `scDblFinder` was run without cluster mode using the doublet rate calculation as implemented in `Demuxafy` [36]. Cells that were identified as doublets by either `vireo` or `demuxmix` (for longitudinal samples only) were filtered out. Cells that were classified as doublets by *both* `scds` and `scDblFinder` were also filtered out.

As significantly more cells were confidently assigned to donors using genetic demultiplexing, the genetic assignments were used in the downstream analysis for most cells; HTO assignments were used for cells from longitudinal samples. As the vast majority of genetic assignments corresponded to a single HTO, these were used to match each cell's genetic assignment to the sample information.

Ambient RNA contamination was removed using `decontX` (1.0.0) [37] including the raw Cell Ranger counts as background.

Clustering and cell type annotation

The 196,687 remaining droplets were then annotated with cell type labels from the Human Lung Cell Atlas v2 (HLCA) using the `RunAzimuth` function from the `azimuth` (0.4.6) GitHub package. The annotated cells were divided into 3 separate data subsets based on their HLCA level 3 labels: 151,349 macrophage cells, 15,511 T/NK cells and the remaining 29,827 "rare" cells. The "rare" cells contained many cells with less than 250 reads after ambient RNA contamination, which were excluded from subsequent analysis.

All data normalisation, integration and clustering was performed using functions from the `Seurat` (4.4.0) CRAN package [38-40]. For each data subset, the cell cycle scores were assigned to each cell using the `CellCycleScoring` function using the inbuilt G2/M and S phase markers. Based on the "Alternate Workflow" in the `Seurat` "Cell-Cycle Scoring and Regression" vignette (https://satijalab.org/seurat/articles/cell_cycle_vignette.html), the difference between the G2/M and S phase scores was calculated to maintain separation of non-cycling cells and cycling cells. The data subsets were then independently normalised using the `Seurat` `SCTransform` (0.4.1) function [41,42], regressing out the G2/M and S phase difference.

The RNA data for each cell type group was then integrated using reciprocal principal components analysis (RPCA) with 30 dimensions and 3000 features. For the T/NK and "rare" cells data, 20 neighbours were used for anchor selection (k.anchor) The number of neighbours to consider when weighting anchors (k.weight) was set to the minimum of 100 and the smallest number of cells in a single sample minus 5. For the macrophage data, default values were used for these parameters.

For the ADT data from the T/NK and "rare" subsets (excluding cells from the "scRNA-seq" experiment), all 163 ADTs were designated as variable features and the data was normalised using the centred log ratio (CLR) normalisation with margin=2. The data was then integrated using canonical correlation analysis (CCA) with 30 dimensions. Any HLA, immunoglobulin, ribosomal and mitochondrial genes were then removed from the variable features, followed by dimensionality reduction and clustering using weighted-nearest neighbor (WNN) analysis

incorporating both the RNA and ADT data using the smart local moving (SLM) algorithm, with up to 30 principal components for RNA and 10 for ADT. Ten resolutions between 0.1 and 1 were explored using the `clustree` CRAN package (0.5.1) [43]. A resolution of 0.6 was used in downstream analysis for T/NK and "rare" cells. This integrated and clustered data was then used as a reference that the previously excluded "scRNA-seq" cells were mapped to using the `MapQuery` function from `Seurat`, allowing for transfer of cluster labels. A combined Uniform Manifold Approximation and Projection (UMAP) was then computed.

The macrophage data was also clustered using the SLM algorithm in `Seurat`, however, only the RNA data was used for clustering due to a lack of sufficiently informative ADTs for distinguishing macrophage subtypes. As previously described, a series of resolutions was examined and 0.6 was selected. The quality of the clusters in each data subset was assessed by examining their Azimuth prediction score distributions, total UMI count distributions and the distributions of the total number of unique genes detected.

Marker gene analysis was performed for each cluster, in each data subset, as described in Sim et al 2021 [44]; log fold change cutoffs of 0.25, 0.25 and 0.5 were used in the `limma`(3.58.1) [45], `treat` [46] test for T/NK, "rare" and macrophage cells, respectively. Gene set enrichment analysis of the REACTOME gene sets (https://www.gsea-msigdb.org/gsea/msigdb/collections.jsp) was performed for each cluster in each data subset using `cameraPR` [47] from the `limma` Bioconductor package.

The ADT data from the "CITE-seq" experiment was normalised using the `dsb` method (1.0.3) [48], including isotype controls. The top ADT markers for each cluster were then identified as described above with a log fold change cutoff of 0.1 used in the `treat` test. Manual inspection of the top marker genes, ADTs and REACTOME pathways for each cluster was used to assign them cellular and/or functional identities. Clusters that shared the same manually assigned label were merged. The marker genes for the finalised clusters were identified using the `FindAllMarkers` `Seurat` function.

Differential expression analysis

Pseudobulk samples were created by summing the counts of cell type for each sample using the `aggregateAcrossCells` function from the `scuttle`(1.12.0)[49] Bioconductor package. Pseudobulk samples with fewer than 500 cells for total macrophages, 50 cells for macrophage subtypes and 25 cells for T/NK and "rare" groups were excluded. Only cell types with

sufficient samples remaining were analysed for differential gene expression between disease conditions.

Any genes with zero counts across all pseudobulk samples were filtered out, as were genes without Entrez identifiers and those with low median $\log_2$ counts per million (CPM). To estimate the unwanted variation present in the data, factor analysis of "negative control features" was performed using the `RUVg` function from the `RUVseq`(1.36.0) [50] Bioconductor package. The set of 3,804 human housekeeping genes published by [51] and provided in the `scMerge`(1.18.0) [52]. Bioconductor package were used as "negative control features". Following dispersion estimation, generalized log-linear models were fitted to the counts for each gene using `edgeR`(4.0.15) [53], taking into account longitudinal samples and *k* components of unwanted variation estimated by `RUVg`, as well as the $\log_2$ of the age and the sex of each sample. The value of *k* for each analysis within a cell type was empirically determined by assessing a combination of relative log expression (RLE) and PCA plots, and p-value histograms. The Non-CF control samples were excluded from the data for the analysis of the effects of CF modifier therapy and bronchiectasis, and an additional factor for the presence of the most clinically significant microorganisms was included. Differentially expressed genes (DEG) were identified using likelihood ratio tests. As the full list of differentially expressed genes was too long to present in its entirety in Figure 3, a 'treat' test [46] with lfc=$\log_2(1.1)$ was also applied. The Benjamini-Hochberg method [54] was used to adjust for multiple testing and genes with a false discovery rate (FDR) < 0.05 were deemed statistically significant.

Gene set and functional pathway analysis

The `goana` function from the `limma` Bioconductor package was used to test statistically significant DEGs for over-representation of gene sets. Gene sets of interest included GO, HALLMARK, REACTOME and WIKIPATHWAYS collections (v2024.1) from the Broad Institute Molecular Signatures Database [55-57]. A list of gene sets specifically relevant to pulmonary fibrosis was also compiled and included the "defective CFTR causes cystic fibrosis" set from REACTOME, the "lung fibrosis" and "nitric oxide metabolism in cystic fibrosis" sets from WIKIPATHWAYS, a "fibrosis transcriptional signature" published by Reyfman et al 2019 [58] and "pulmonary fibrosis ctd", which is the set of genes with direct evidence relating to pulmonary fibrosis from the Comparative Toxicogenomics Database [59]. Multiple testing adjustment was performed using the Benjamini-Hochberg method [54]. All of

the gene sets described were also tested using a functional class scoring approach with the `cameraPR` function from the `limma` Bioconductor package. Gene sets with an FDR < 0.05 were considered statistically significant.

Statistical analysis of cell type proportions

Cell type proportions were calculated using the `speckle` (1.2.0) function `propeller` [60], based on our broad (ann_level_1) and fine (ann_level_3) annotations, and were arcsine transformed. The transformed proportions were analysed for associations with disease conditions using the `limma` Bioconductor package. Briefly, linear models were fitted to the data, taking into account batch, $\log_2$ of the age, and sex for each sample. A random effect was also included to account for longitudinal samples using the `duplicateCorrelation` function from `limma`. Empirical Bayes moderated t-tests with robust=TRUE [61] were used to identify significant changes in cell type proportion with disease condition. As above, the Benjamini-Hochberg method was used to adjust for false discovery rate [54]. Cell types with FDR < 0.05 were considered statistically significant.

FIGURE LEGENDS

Figure 1. An immune and epithelial cell atlas of early life BAL. (A) Overview of study cohort and experimental workflow. (B) UMAP depicting the broad immune and epithelial cell populations identified in early life BAL; based on dimension reduction of gene expression data only. (C) Bar plots depicting total cell numbers for each BAL sample (top), and the proportion of each broad cell type within each BAL sample (bottom), separated by treatment and disease groups. (D) Dot plot depicting marker genes of each identified broad immune and epithelial cell population. (E) Heatmap depicting protein (antibody derived tag (ADT)) expression on each identified broad immune and epithelial cell population. DSB refers to normalised ADT expression using DSB method (see methods).

Figure 2. Sub-clustering analysis reveals heterogeneity within BAL macrophages, T cells, myeloid cells, and other rare cell populations. UMAP depicting sub-clustering analysis of BAL macrophages; based on dimension reduction of gene expression data only. (B) Dot plot depicting marker genes of each identified macrophage subpopulation. (C) Stacked bar plot depicting the proportion of each macrophage subpopulation in each BAL sample, separated by treatment and disease groups. (D) UMAP depicting sub-clustering analysis of BAL T/NK cells; based on dimension reduction of gene expression and ADT data. (E) Dot plot depicting marker genes of each identified T/NK cell subpopulation. (F) Stacked bar plot depicting the proportion of each T/NK cell subpopulation in each BAL sample, separated by treatment and disease groups. (G) UMAP depicting sub-clustering analysis of BAL myeloid and rare cell populations; based on dimension reduction of gene expression and ADT data. (H) Dot plot depicting marker genes of each identified myeloid/rare cell subpopulation. (I) Stacked bar plot depicting the proportion of each myeloid/rare subpopulation in each BAL sample, separated by treatment and disease groups.

Figure 3. Widespread dysregulation of BAL macrophage responses in preschool children with CF compared to non-CF controls. (A) Proportions of CD4 Tregs, monocytes, NK-T cells, and macro-IGF1 cells in BAL samples from children with CF (no modulator) (n=25) and non-CF controls (n=8). *indicates significant FDR adjusted p-value. (B) Summary of the number of differentially expressed genes between CF (no modulator) (CF.NO_MOD) and non-CF control groups for each tested macrophage subpopulation. (C) Heatmap depicting the most significant differentially expressed genes between CF (no modulator) (CF.NO_MOD) and non-CF control groups for each tested macrophage subpopulation. “Multiple” refers to whether the gene was differentially expressed in multiple

macrophage subpopulations (FALSE = differentially expressed only in one macrophage subpopulation, TRUE = differentially expressed in multiple macrophage subpopulations). (D) Volcano plot depicting up- and down-regulated genes in the CF (no modulator) (CF.NO_MOD) and non-CF comparison within the total macrophage pool. (E) REACTOME pathway analysis of differentially expressed genes within the macro-alveolar, macro-CCL, macro-lipid and macro-monocyte-derived populations. (F) HALLMARK pathway analysis of differentially expressed genes within the macro-alveolar and macro-monocyte-derived populations. (G) Lung fibrosis pathway analysis of differentially expressed genes within the total macrophage and macro-alveolar populations.

Figure 4. BAL macrophage transcriptional signatures are associated with CF bronchiectasis. (A) Proportions of CD4 T-IFN and HSP+ B cells in BAL samples from CF children with bronchiectasis (CF.NO_MOD.S, “CF severe”) (n=8) and no bronchiectasis (CF.NO_MOD.M, “CF mild”) (n=17). (B) Summary of the number of differentially expressed genes between CF severe and CF mild groups for each tested macrophage subpopulation. (C) Heatmap depicting genes that were differentially expressed in multiple macrophage subpopulations between CF severe and CF mild groups.

Figure 5. The CFTR modulator ivacaftor modifies BAL macrophage function in early life. (A) Proportions of NK-T cells, CD4 T-IFN, and monocytes in BAL samples from children treated with ivacaftor (CF.IVA) (n=8), CF.NO_MOD (n=25) and non.CF controls (n=8). (B) Proportions of NK- T cells, CD4 T-IFN, CD4 T-reg, monocytes and macro-CCL in BAL samples from children treated with lumacaftor/ivacaftor (CF.LUMA_IVA) (n=4), CF.NO_MOD (n=25) and non.CF controls (n=8). (C) Summary of the number of differentially expressed genes between CF.IVA (n=8) and CF (no modulator) (CF.NO_MOD) (n=25) for each tested macrophage subpopulation. (D) Heatmap depicting the most significant differentially expressed genes between CF.IVA and CF (no modulator) (CF.NO_MOD) groups for each tested macrophage subpopulation. “Multiple” refers to whether the gene was differentially expressed in multiple macrophage subpopulations (FALSE = differentially expressed only in one macrophage subpopulation, TRUE = differentially expressed in multiple macrophage subpopulations). (E) Volcano plot depicting up- and down-regulated genes in the CF.IVA and CF (no modulator) (CF.NO_MOD) comparison within the total macrophage pool. (F) HALLMARK and REACTOME pathway analysis of differentially expressed genes within the macro-alveolar population. (G) Gene ontology and REACTOME pathway analysis revealing remodelling of neutrophil response

pathways in the macro-alveolar population. (H) Selected differentially expressed genes related to neutrophil pathways within the macro-alveolar population in CF.IVA and CF (no modulator) (CF.NO_MOD) comparison (all FDR $p<0.05$).

REFERENCES

1. Shanthikumar, S., Stick, S.M. & Ranganathan, S.C. Minimal structural lung disease in early life represents significant pathology. *Journal of Cystic Fibrosis* **20**, e118-e120 (2021).
2. Mall, M.A.*, et al.* Neutrophil serine proteases in cystic fibrosis: role in disease pathogenesis and rationale as a therapeutic target. *Eur Respir Rev* **33**(2024).
3. Rosenow, T.*, et al.* The cumulative effect of inflammation and infection on structural lung disease in early cystic fibrosis. *European Respiratory Journal* **54**, 1801771 (2019).
4. Casey, M.*, et al.* Effect of elexacaftor/tezacaftor/ivacaftor on airway and systemic inflammation in cystic fibrosis. *Thorax* **78**, 835-839 (2023).
5. Sly, P.D.*, et al.* Risk factors for bronchiectasis in children with cystic fibrosis. *The New England journal of medicine* **368**, 1963-1970 (2013).
6. Loske, J.*, et al.* Pharmacological Improvement of Cystic Fibrosis Transmembrane Conductance Regulator Function Rescues Airway Epithelial Homeostasis and Host Defense in Children with Cystic Fibrosis. *American journal of respiratory and critical care medicine* **209**, 1338-1350 (2024).
7. Madissoon, E.*, et al.* A spatially resolved atlas of the human lung characterizes a gland-associated immune niche. *Nat Genet* **55**, 66-77 (2023).
8. Sikkema, L.*, et al.* An integrated cell atlas of the lung in health and disease. *Nature Medicine* **29**, 1563-1577 (2023).
9. Li, X.*, et al.* ScRNA-seq expression of IFI27 and APOC2 identifies four alveolar macrophage superclusters in healthy BALF. *Life Sci Alliance* **5**(2022).
10. Oakley, M.S.*, et al.* TCRβ-expressing macrophages induced by a pathogenic murine malaria correlate with parasite burden and enhanced phagocytic activity. *PLoS One* **13**, e0201043 (2018).
11. Rodriguez-Cruz, A.*, et al.* CD3(+) Macrophages Deliver Proinflammatory Cytokines by a CD3- and Transmembrane TNF-Dependent Pathway and Are Increased at the BCG-Infection Site. *Frontiers in immunology* **10**, 2550 (2019).
12. Burel, J.G.*, et al.* Circulating T cell-monocyte complexes are markers of immune perturbations. *Elife* **8**(2019).
13. Yang, M.*, et al.* Cytokine storm promoting T cell exhaustion in severe COVID-19 revealed by single cell sequencing data analysis. *Precis Clin Med* **5**, pbac014 (2022).
14. Wing, E.*, et al.* Double-negative-2 B cells are the major synovial plasma cell precursor in rheumatoid arthritis. *Frontiers in immunology* **14**, 1241474 (2023).
15. Januska, M.N. & Walsh, M.J. Single-Cell RNA Sequencing Reveals New Basic and Translational Insights in the Cystic Fibrosis Lung. *American journal of respiratory cell and molecular biology* **68**, 131-139 (2023).
16. Shanthikumar, S., Burton, M., Saffery, R., Ranganathan, S.C. & Neeland, M.R. Single-Cell Flow Cytometry Profiling of BAL in Children. *American journal of respiratory cell and molecular biology* **63**, 152-159 (2020).
17. Jaudas, F.*, et al.* Perinatal dysfunction of innate immunity in cystic fibrosis. *Science translational medicine* **17**, eadk9145 (2025).
18. Schupp, J.C.*, et al.* Single-Cell Transcriptional Archetypes of Airway Inflammation in Cystic Fibrosis. *American journal of respiratory and critical care medicine* **202**, 1419-1429 (2020).
19. Gaggar, A.*, et al.* The role of matrix metalloproteinases in cystic fibrosis lung disease. *European Respiratory Journal* **38**, 721-727 (2011).
20. Bühling, F.*, et al.* Pivotal role of cathepsin K in lung fibrosis. *Am J Pathol* **164**, 2203-2216 (2004).
21. Pardo, A., Cabrera, S., Maldonado, M. & Selman, M. Role of matrix metalloproteinases in the pathogenesis of idiopathic pulmonary fibrosis. *Respiratory research* **17**, 23 (2016).

22. Chen, H.M.*, et al.* Blocking immunoinhibitory receptor LILRB2 reprograms tumor-associated myeloid cells and promotes antitumor immunity. *J Clin Invest* **128**, 5647-5662 (2018).
23. Shanthikumar, S., Ranganathan, S. & Neeland, M.R. Ivacaftor, not ivacaftor/lumacaftor, associated with lower pulmonary inflammation in preschool cystic fibrosis. *Pediatric pulmonology* **57**, 2549-2552 (2022).
24. Shanthikumar, S.*, et al.* Inflammation in preschool cystic fibrosis is of mixed phenotype, extends beyond the lung and is differentially modified by CFTR modulators. *Thorax* (2025).
25. Shanthikumar, S. & Massie, J. A Review of Treatments That Improve Cystic Fibrosis Transmembrane Conductance Regulator Function. *Clinical Medicine Insights: Therapeutics* **9**, 1179559X17719123 (2017).
26. Quon, B.S. & Rowe, S.M. New and emerging targeted therapies for cystic fibrosis. *Bmj* **352**, i859 (2016).
27. Shivanthan Shanthikumar, L.G., Melanie R Neeland Processing of pediatric bronchoalveolar lavage samples for single cell analysis v3. *protocols.io* (2024).
28. Blischak, J.D., Carbonetto, P. & Stephens, M. Creating and sharing reproducible research code the workflowr way. *F1000Research* **8**, 1749 (2019).
29. Maksimovic, J.*, et al.* Single-cell atlas of bronchoalveolar lavage from preschool cystic fibrosis reveals new cell phenotypes. *bioRxiv*, 2022.2006.2017.496207 (2022).
30. Lun, A.T.L.*, et al.* EmptyDrops: distinguishing cells from empty droplets in droplet-based single-cell RNA sequencing data. *Genome Biol* **20**, 63 (2019).
31. Klein, H.U. demuxmix: Demultiplexing oligonucleotide-barcoded single-cell RNA sequencing data with regression mixture models. *bioRxiv* (2023).
32. Huang, X. & Huang, Y. Cellsnp-lite: an efficient tool for genotyping single cells. *Bioinformatics* **37**, 4569-4571 (2021).
33. Huang, Y., McCarthy, D.J. & Stegle, O. Vireo: Bayesian demultiplexing of pooled single-cell RNA-seq data without genotype reference. *Genome Biol* **20**, 273 (2019).
34. Bais, A.S. & Kostka, D. scds: computational annotation of doublets in single-cell RNA sequencing data. *Bioinformatics* **36**, 1150-1158 (2020).
35. Germain, P.L., Lun, A., Garcia Meixide, C., Macnair, W. & Robinson, M.D. Doublet identification in single-cell sequencing data using scDblFinder. *F1000Research* **10**, 979 (2021).
36. Neavin, D.*, et al.* Demuxafy: improvement in droplet assignment by integrating multiple single-cell demultiplexing and doublet detection methods. *Genome Biol* **25**, 94 (2024).
37. Yang, S.*, et al.* Decontamination of ambient RNA in single-cell RNA-seq with DecontX. *Genome Biol* **21**, 57 (2020).
38. Hao, Y.*, et al.* Integrated analysis of multimodal single-cell data. 2020.2010.2012.335331 (2020).
39. Butler, A., Hoffman, P., Smibert, P., Papalexi, E. & Satija, R. Integrating single-cell transcriptomic data across different conditions, technologies, and species. *Nat Biotechnol* **36**, 411-420 (2018).
40. Stuart, T.*, et al.* Comprehensive Integration of Single-Cell Data. *Cell* **177**, 1888-1902.e1821 (2019).
41. Choudhary, S. & Satija, R. Comparison and evaluation of statistical error models for scRNA-seq. *Genome Biol* **23**, 27 (2022).
42. Hafemeister, C. & Satija, R. Normalization and variance stabilization of single-cell RNA-seq data using regularized negative binomial regression. *Genome Biol* **20**, 296 (2019).
43. Zappia, L. & Oshlack, A. Clustering trees: a visualization for evaluating clusterings at multiple resolutions. *GigaScience* **7**(2018).
44. Sim, C.B.*, et al.* Sex-Specific Control of Human Heart Maturation by the Progesterone Receptor. *Circulation* (2021).

45. Ritchie, M.E., *et al.* limma powers differential expression analyses for RNA-sequencing and microarray studies. *Nucleic acids research* **43**, e47 (2015).
46. McCarthy, D.J. & Smyth, G.K. Testing significance relative to a fold-change threshold is a TREAT. *Bioinformatics* **25**, 765-771 (2009).
47. Wu, D. & Smyth, G.K. Camera: a competitive gene set test accounting for inter-gene correlation. *Nucleic acids research* **40**, e133 (2012).
48. Mulè, M.P., Martins, A.J. & Tsang, J.S. Normalizing and denoising protein expression data from droplet-based single cell profiling. *Nat Commun* **13**, 2099 (2022).
49. McCarthy, D.J., Campbell, K.R., Lun, A.T. & Wills, Q.F. Scater: pre-processing, quality control, normalization and visualization of single-cell RNA-seq data in R. *Bioinformatics* **33**, 1179-1186 (2017).
50. Risso, D., Ngai, J., Speed, T.P. & Dudoit, S. Normalization of RNA-seq data using factor analysis of control genes or samples. *Nat Biotechnol* **32**, 896-902 (2014).
51. Eisenberg, E. & Levanon, E.Y. Human housekeeping genes, revisited. *Trends Genet* **29**, 569-574 (2013).
52. Lin, Y., *et al.* scMerge leverages factor analysis, stable expression, and pseudoreplication to merge multiple single-cell RNA-seq datasets. *Proc Natl Acad Sci U S A* **116**, 9775-9784 (2019).
53. Robinson, M.D., McCarthy, D.J. & Smyth, G.K. edgeR: a Bioconductor package for differential expression analysis of digital gene expression data. *Bioinformatics* **26**, 139-140 (2010).
54. Benjamini, Y. & Hochberg, Y. Controlling the False Discovery Rate - a Practical and Powerful Approach to Multiple Testing. *J R Stat Soc B* **57**, 289-300 (1995).
55. Liberzon, A., *et al.* The Molecular Signatures Database (MSigDB) hallmark gene set collection. *Cell Syst* **1**, 417-425 (2015).
56. Liberzon, A., *et al.* Molecular signatures database (MSigDB) 3.0. *Bioinformatics* **27**, 1739-1740 (2011).
57. Subramanian, A., *et al.* Gene set enrichment analysis: a knowledge-based approach for interpreting genome-wide expression profiles. *Proc Natl Acad Sci U S A* **102**, 15545-15550 (2005).
58. Reyfman, P.A., *et al.* Single-Cell Transcriptomic Analysis of Human Lung Provides Insights into the Pathobiology of Pulmonary Fibrosis. *American journal of respiratory and critical care medicine* **199**, 1517-1536 (2019).
59. Davis, A.P., *et al.* Comparative Toxicogenomics Database's 20th anniversary: update 2025. *Nucleic acids research* **53**, D1328-d1334 (2025).
60. Phipson, B., *et al.* propeller: testing for differences in cell type proportions in single cell data. *Bioinformatics* **38**, 4720-4726 (2022).
61. Phipson, B., Lee, S., Majewski, I.J., Alexander, W.S. & Smyth, G.K. ROBUST HYPERPARAMETER ESTIMATION PROTECTS AGAINST HYPERVARIABLE GENES AND IMPROVES POWER TO DETECT DIFFERENTIAL EXPRESSION. *Ann Appl Stat* **10**, 946-963 (2016).

A
45 BAL samples
(children aged 0.5-8 years)
cystic fibrosis
(n=37)
non-CF control
(n=8)
CF (no modulator)
(n=25)
CF (ivacaftor)
(n=8)
CF (lumacaftor/ivacaftor)
(n=4)
Single-cell RNA sequencing +
Antibody derived tags (ADT)
194 407 high quality cells for
downstream analysis
B
proliferating macrophages
neutrophils
dividing innate cells
DC cells
monocytes
mast cells
epithelial cells
macrophages
NK cells
gamma delta T cells
NK-T cells
proliferating T/NK
CD8 T cells
innate lymphocyte
CD4 T cells
B cells
C
Number of cells
Cell type proportion
Sample
Condition
CF.IVA
CF.LUMA_IVA
CF.NO_MOD
NON_CF.CTRL
Cell type
B cells
CD4 T cells
CD8 T cells
DC cells
dividing innate cells
epithelial cells
gamma delta T cells
innate lymphocyte
macrophages
mast cells
monocytes
neutrophils
NK cells
NK-T cells
proliferating macrophages
proliferating T/NK
D
MS4A1
JCHAIN
CD79A
LTB
POU2F2
IL32
CD2
TRAC
KLRB1
CCL5
GNLY
GZMA
NKG7
CCL17
GPR183
C15orf48
RGS1
LGALS2
TOP2A
PCLAF
MKI67
UBE2C
TYMS
SCGB3A1
WFDC2
SLPI
LCN2
CAPS
TRDC
FTL
APOC1
FTH1
APOE
C1QA
TPSAB1
TPSB2
MS4A2
SLC18A2
LIF
VCAN
FCGR2B
CLEC10A
FGL2
FCN1
VEGFA
SERPINB9
APOBEC3A
CD300E
CD7
XCL2
XCL1
TNFRSF9
TNFRSF18
STMN1
TUBB
CENPF
HMGN2
Average Expression
Percent Expressed
E
Protein
Cell type
ADT Exp.
CD11b
CD11c
CD14
CD172a (SIRPα)
CD19
CD1c
CD20
CD3
CD33
CD35
CD4
CD45
CD48
CD49b
CD55
CD56 (NCAM)
CD63
CD71
CD8
CLEC12A
FcεRIα
IgE
TCR Vδ2

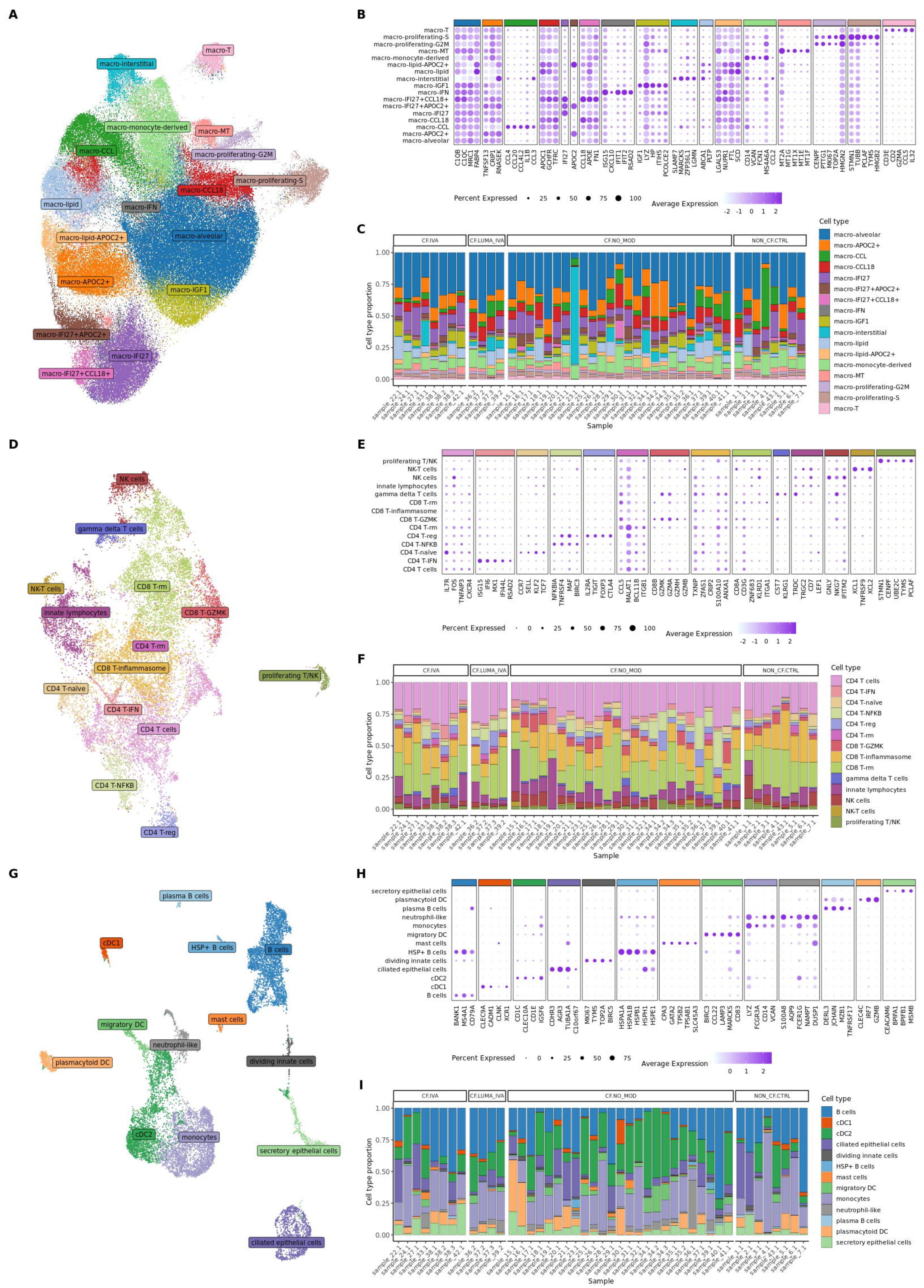
A
macro-T
macro-interstitial
macro-monocyte-derived
macro-MT
macro-CCL
macro-proliferating-G2M
macro-proliferating-S
macro-CCL18
macro-lipid
macro-IFN
macro-alveolar
macro-lipid-APOC2+
macro-APOC2+
macro-IGF1
macro-IFI27+APOC2+
macro-IFI27
macro-IFI27+CCL18+
B
Percent Expressed
Average Expression
C
CF.IVA
CF.LUMA_IVA
CF.NO_MOD
NON_CF.CTRL
Cell type proportion
Sample
Cell type
D
NK cells
gamma delta T cells
NK-T cells
CD8 T-rm
innate lymphocytes
CD8 T-GZMK
CD4 T-rm
CD8 T-inflammasome
proliferating T/NK
CD4 T-naïve
CD4 T-IFN
CD4 T cells
CD4 T-NFKB
CD4 T-reg
E
F
G
plasma B cells
cDC1
HSP+ B cells
B cells
mast cells
migratory DC
neutrophil-like
plasmacytoid DC
dividing innate cells
cDC2
monocytes
secretory epithelial cells
ciliated epithelial cells
H
I

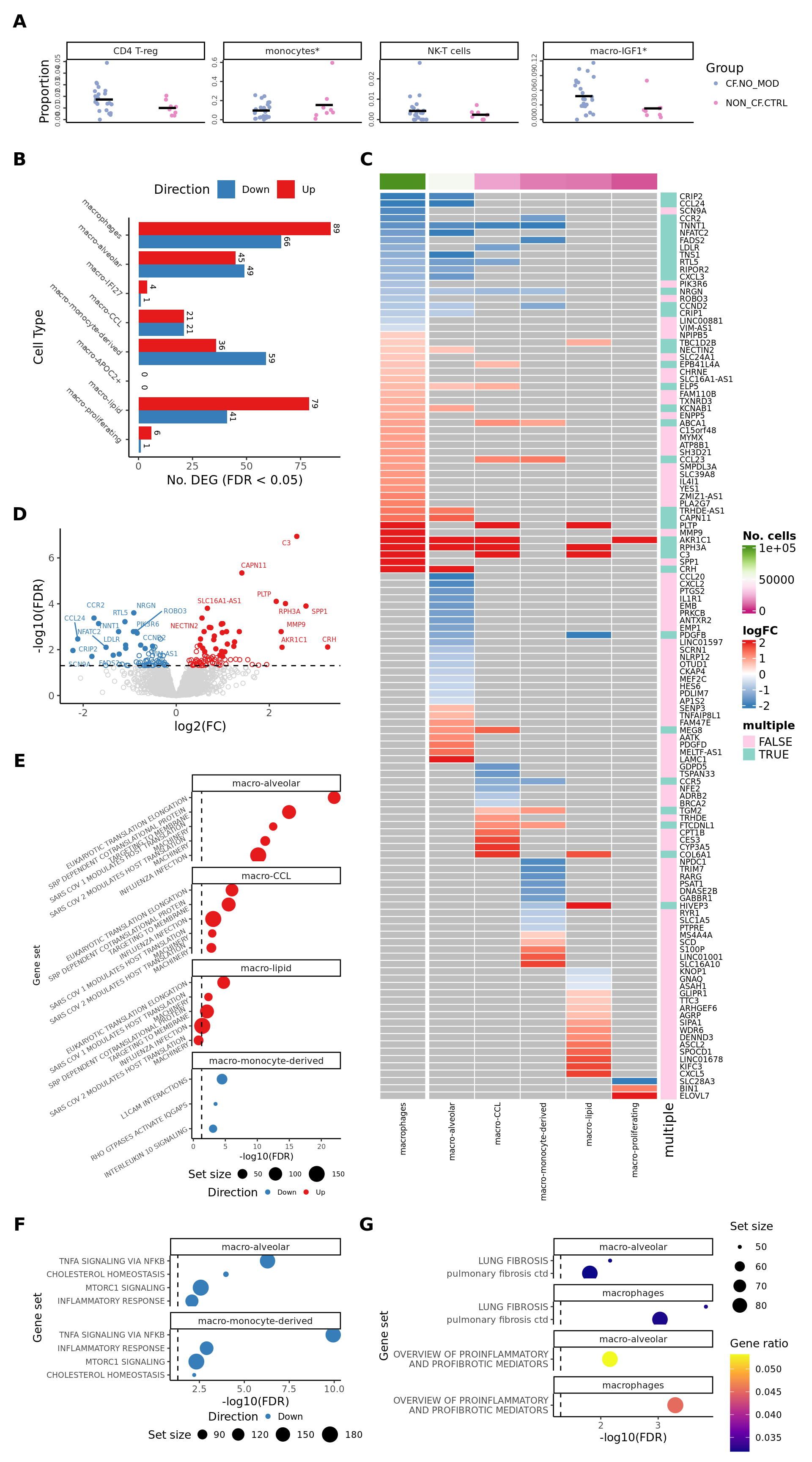
A
CD4 T-reg
monocytes*
NK-T cells
macro-IGF1*
Proportion
Group
CF.NO_MOD
NON_CF.CTRL
B
Direction
Down
Up
Cell Type
macrophages
macro-alveolar
macro-IFI27
macro-CCL
macro-monocyte-derived
macro-APOC2+
macro-lipid
macro-proliferating
No. DEG (FDR < 0.05)
C
No. cells
logFC
multiple
FALSE
TRUE
macrophages
macro-alveolar
macro-CCL
macro-monocyte-derived
macro-lipid
macro-proliferating
multiple
D
-log10(FDR)
log2(FC)
E
macro-alveolar
macro-CCL
macro-lipid
macro-monocyte-derived
Gene set
EUKARYOTIC TRANSLATION ELONGATION
SRP DEPENDENT COTRANSLATIONAL PROTEIN TARGETING TO MEMBRANE
SARS COV 1 MODULATES HOST TRANSLATION MACHINERY
SARS COV 2 MODULATES HOST TRANSLATION MACHINERY
INFLUENZA INFECTION
L1CAM INTERACTIONS
RHO GTPASES ACTIVATE IQGAPS
INTERLEUKIN 10 SIGNALING
-log10(FDR)
Set size
Direction
Down
Up
F
macro-alveolar
macro-monocyte-derived
Gene set
TNFA SIGNALING VIA NFKB
CHOLESTEROL HOMEOSTASIS
MTORC1 SIGNALING
INFLAMMATORY RESPONSE
-log10(FDR)
Direction
Down
Set size
G
macro-alveolar
macrophages
Gene set
LUNG FIBROSIS
pulmonary fibrosis ctd
OVERVIEW OF PROINFLAMMATORY AND PROFIBROTIC MEDIATORS
-log10(FDR)
Set size
Gene ratio

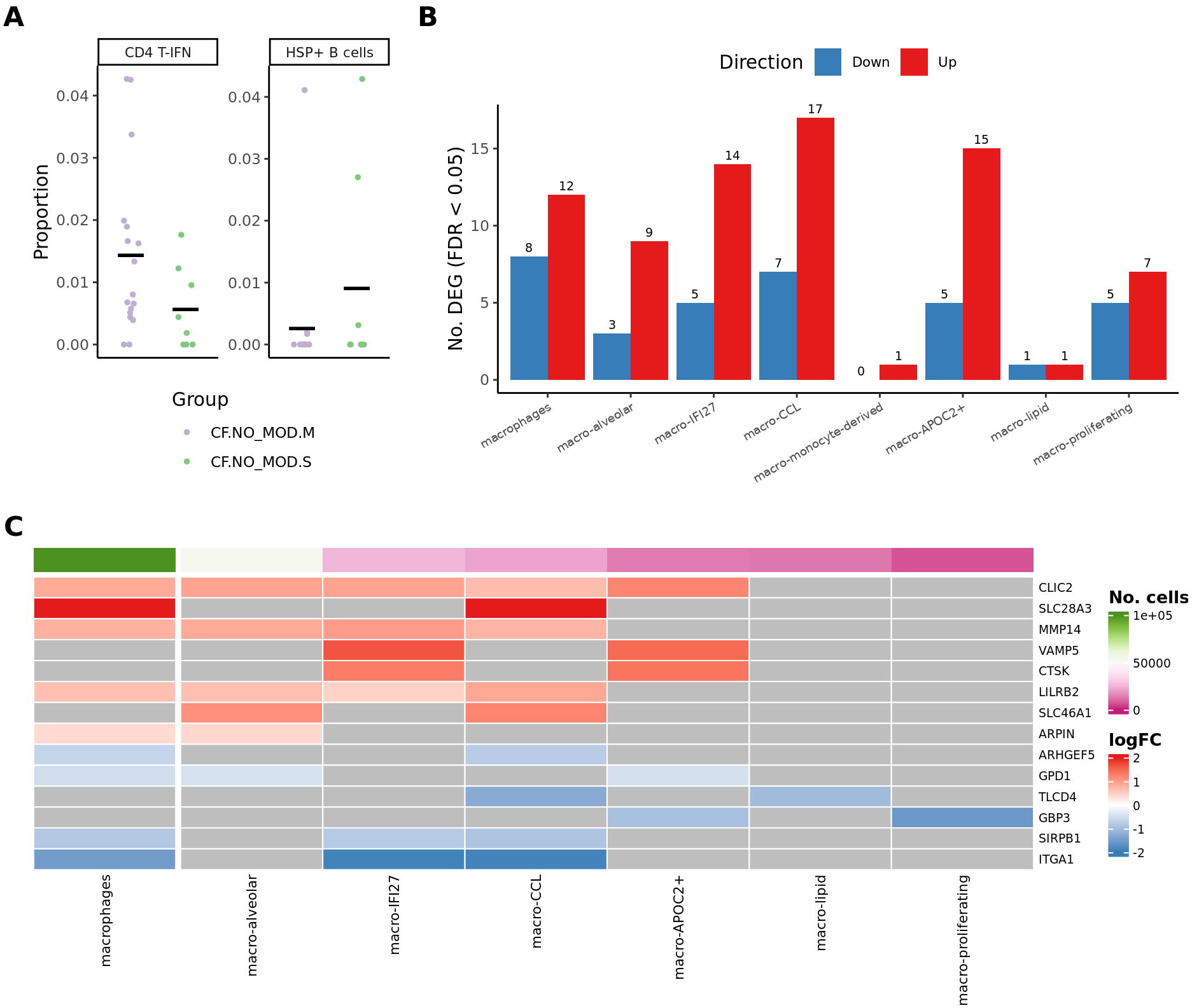
A
CD4 T-IFN
HSP+ B cells
Proportion
0.04
0.03
0.02
0.01
0.00
Group
CF.NO_MOD.M
CF.NO_MOD.S
B
Direction
Down
Up
No. DEG (FDR < 0.05)
macrophages
macro-alveolar
macro-IFI27
macro-CCL
macro-monocyte-derived
macro-APOC2+
macro-lipid
macro-proliferating
C
CLIC2
SLC28A3
MMP14
VAMP5
CTSK
LILRB2
SLC46A1
ARPIN
ARHGEF5
GPD1
TLCD4
GBP3
SIRPB1
ITGA1
No. cells
1e+05
50000
0
logFC
2
1
0
-1
-2

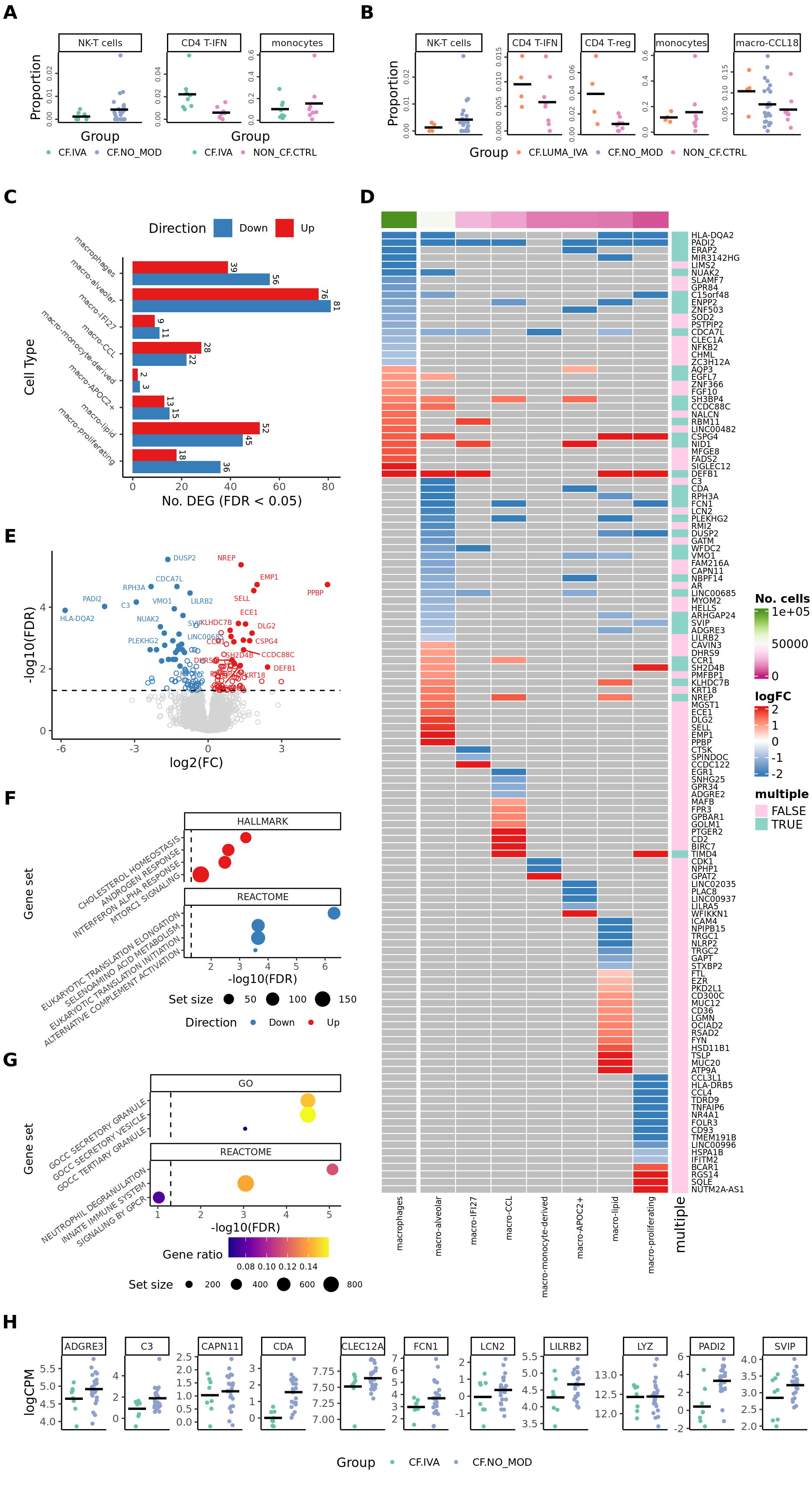
A
NK-T cells
CD4 T-IFN
monocytes
Proportion
Group
CF.IVA
CF.NO_MOD
NON_CF.CTRL
B
NK-T cells
CD4 T-IFN
CD4 T-reg
monocytes
macro-CCL18
Proportion
Group
CF.LUMA_IVA
CF.NO_MOD
NON_CF.CTRL
C
Direction
Down
Up
Cell Type
macrophages
macro-alveolar
macro-IFI27
macro-CCL
macro-monocyte-derived
macro-APOC2+
macro-lipid
macro-proliferating
No. DEG (FDR < 0.05)
D
HLA-DQA2
PADI2
ERAP2
MIR3142HG
LIMS2
NUAK2
SLAMF7
GPR84
C15orf48
ENPP2
ZNF503
SOD2
PSTPIP2
CDCA7L
CLEC1A
NFKB2
CHML
ZC3H12A
AQP3
EGFL7
ZNF366
FGF10
SH3BP4
CCDC88C
NALCN
RBM11
LINC00482
CSPG4
NID1
MFGE8
FADS2
SIGLEC12
DEFB1
C3
CDA
RPH3A
FCN1
LCN2
PLEKHG2
RMI2
DUSP2
GATM
WFDC2
VMO1
FAM216A
CAPN11
NBPF14
AR
LINC00685
MYOM2
HELLS
ARHGAP24
SVIP
ADGRE3
LILRB2
CAVIN3
DHRS9
CCR1
SH2D4B
PMFBP1
KLHDC7B
KRT18
NREP
MGST1
ECE1
DLG2
SELL
EMP1
PPBP
CTSK
SPINDOC
CCDC122
EGR1
SNHG25
GPR34
ADGRE2
MAFB
FPR3
GPBAR1
GOLM1
PTGER2
CD2
BIRC7
TIMD4
CDK1
NPHP1
GPAT2
LINC02035
PLAC8
LINC00937
LILRA5
WFIKKN1
ICAM4
NPIPB15
TRGC1
NLRP2
TRGC2
GAPT
STXBP2
FTL
EZR
PKD2L1
CD300C
MUC12
CD36
LGMN
OCIAD2
RSAD2
FYN
HSD11B1
TSLP
MUC20
ATP9A
CCL3L1
HLA-DRB5
CCL4
TDRD9
TNFAIP6
NR4A1
FOLR3
CD93
TMEM191B
LINC00996
HSPA1B
IFITM2
BCAR1
RGS14
SQLE
NUTM2A-AS1
macrophages
macro-alveolar
macro-IFI27
macro-CCL
macro-monocyte-derived
macro-APOC2+
macro-lipid
macro-proliferating
multiple
No. cells
1e+05
50000
0
logFC
2
1
0
-1
-2
multiple
FALSE
TRUE
E
-log10(FDR)
log2(FC)
DUSP2
NREP
CDCA7L
EMP1
RPH3A
PPBP
PADI2
C3
VMO1
LILRB2
SELL
HLA-DQA2
NUAK2
ECE1
KLHDC7B
DLG2
PLEKHG2
LINC00685
CCR1
CSPG4
SH2D4B
CCDC88C
DEFB1
KRT18
F
HALLMARK
CHOLESTEROL HOMEOSTASIS
ANDROGEN RESPONSE
INTERFERON ALPHA RESPONSE
MTORC1 SIGNALING
REACTOME
EUKARYOTIC TRANSLATION ELONGATION
SELENOAMINO ACID METABOLISM
EUKARYOTIC TRANSLATION INITIATION
ALTERNATIVE COMPLEMENT ACTIVATION
Gene set
-log10(FDR)
Set size
50
100
150
Direction
Down
Up
G
GO
GOCC SECRETORY GRANULE
GOCC SECRETORY VESICLE
GOCC TERTIARY GRANULE
REACTOME
NEUTROPHIL DEGRANULATION
INNATE IMMUNE SYSTEM
SIGNALING BY GPCR
Gene set
-log10(FDR)
Gene ratio
0.08 0.10 0.12 0.14
Set size
200
400
600
800
H
ADGRE3
C3
CAPN11
CDA
CLEC12A
FCN1
LCN2
LILRB2
LYZ
PADI2
SVIP
logCPM
Group
CF.IVA
CF.NO_MOD